

the SN images have been measured following two approaches. Pierel et al. (2024) estimated the delay by reconstructing the SN light curves from multi-epoch JWST/NIRCam photometry, making use of the complete surface brightness reconstruction of Arc 2 from the present work. Chen et al. (2024) leveraged JWST/NIRSpec spectroscopy to determine the SN phase via template fitting, from which the time delays could be inferred. In both approaches, values for the absolute magnifications were measured for each of the three SN appearances and used in the H_0 inference (Pascale et al. 2025).

Regardless of the goal—measuring H_0 from the time delays or studying the SN host galaxy—an accurate lens model of the foreground deflector must be constructed first. Recently, Pascale et al. (2025) gathered seven independent teams to perform the strong lens modeling of G165. The same set of cluster members, additional galaxies and lensing constraints was used by all teams. While all models showed overall good fits, the separation between the model-predicted and observed positions across all images varied significantly among the models (from 0''.07 to 1''.1 in rms). Such a spread given the same set of observables should not be surprising, given the variety of modeling assumptions: some models are based on varying numbers of parametric profiles, others are based on regularized mass density grids, and some are a combination of both approaches. Despite the variety in modeling approaches, Agrawal et al. (2025) found that all these seven models of G165 systematically overestimate the magnification of SN H0pe, potentially biasing the inferred H_0 value to the higher side. With additional and better lensing constraints (more multiple image families, more accurate astrometry and redshifts, etc.)—and provided that models are flexible enough—one may expect that different approaches lead to more consistent results. This hypothesis has been recently explored by Perera et al. (2025), although the type of lensing constraints remained limited to *point-like* images, as for the vast majority of cluster-scale lens models.

Some analyses have explored the inclusion of *spatially extended* constraints by explicitly modeling the surface brightness distribution of the arcs. In a galaxy-scale, cluster-hosted lens system, Galan et al. (2024) showed that explicitly modeling the lensed source surface brightness provided meaningful corrections to the original cluster lens model. Over the scale of galaxy groups, extended arcs were used in several analyses such as in Suyu & Halkola (2010), Wang et al. (2022), Bolamperti et al. (2023), Sheu et al. (2024) and Ding et al. (2025) to significantly better constrain the mass distribution of the lensing groups. The reconstruction of extended arcs on cluster scales is scarcer in the literature, in particular due to inherently larger computational costs. However, recently, this long-standing problem started to be addressed. For instance, Acebron et al. (2024) performed the pixelated source modeling of a quasar host galaxy triply lensed by a galaxy cluster, giving new insights on quasar-host relationships at high redshift while significantly improving the lens model precision. In the galaxy cluster hosting the multiply imaged SN Refsdal (Kelly et al. 2015), Schuldt et al. (in prep.) also modeled the full surface brightness of the SN host, finding 1 to 2 orders of magnitude improvements in mass model parameter uncertainties.

Studying the host of Type Ia SNe at redshifts $z \gtrsim 2$ is key to understand their joint evolution over time. Host properties such as stellar mass, star-formation rate and metallicity can all influence the SN luminosities and light-curve shapes (see Ruiter & Seitenzahl 2025, for a recent review). In particular, extinction by dust in the vicinity of SNe and along the line-of-sight directly affects their spectral energy distribution, potentially introduc-

ing biases into distance measurements (e.g., Kelly et al. 2010; Popovic et al. 2024; Meldorf et al. 2023). Therefore, at $z \sim 2$ where galaxies are younger and more metal-poor, such studies are especially important for ensuring the reliability of SNe Ia as standard candles. Additionally, constraining the relationship between the SNe brightness and the size and mass of their host is important to avoid biases in magnitude-based selections of SNe (e.g., Roman et al. 2018; Uddin et al. 2020), a challenge further complicated by lensing magnification for lensed SNe. Studying the environment of the most distant SNe—often revealed by massive strong lenses like clusters—is also key to probe SN progenitors’ age and composition, and better understand the triggering processes of Type Ia explosions and how their rate evolve over time (e.g., Hakobyan et al. 2020; Chakraborty et al. 2024). Specifically for SN H0pe, Frye et al. (2024) presented a NIRCam+NIRSpec spectrophotometric analysis to extract star formation properties and quantified color excess in Arc 2, while Chen et al. (2024) measured dust extinction parameters directly from the NIRSpec spectra.

In the present work, we follow a similar approach as Acebron et al. (2024) using the GLEE modeling code (Suyu & Halkola 2010; Suyu et al. 2012) to incorporate the entire Arc 2 from SN H0pe host in the set of lensing constraints. We discuss the precision improvements on the properties of the two cluster-scale, dark-matter dominated components of this merging cluster. Our extended source model allows us to reconstruct a multi-band image of the SN H0pe host galaxy. Finally, we provide dust extinction maps in both image and source planes of that galaxy revealing the dust environment of SN H0pe and estimate the dust extinction at the SN position. We also compare our results to those of previous analyses (Frye et al. 2024; Pierel et al. 2024; Chen et al. 2024).

When required, we assume a flat Λ cold dark matter cosmology, with $H_0 = 70 \text{ km s}^{-1} \text{ Mpc}^{-1}$, $\Omega_m = 0.3$ and $\Omega_\Lambda = 0.7$. This cosmology leads to angular sizes of $4.9 \text{ kpc arcsec}^{-1}$ at $z = 0.348$ (cluster plane) and $8.4 \text{ kpc arcsec}^{-1}$ at $z = 1.78$ (SN host plane).

This paper is organized as follows. We describe the imaging data of G165 in Sect. 2. We present the results of our point-like only lens model in Sect. 3.1, while results of our improved model including the reconstruction of the SN host are shown in Sect. 3.2. We focus on the properties of the host galaxy and build its dust extinction map in Sect. 4. Finally, we conclude our work in Sect. 5.

2. Data

The data acquisition and reduction is fully described in Frye et al. (2024), and here we give a short summary. G165 was observed by JWST under the PEARLS programm (ID 1176, P.I. R. Windhorst) in March 2023 with NIRCam. Additional NIRCam imaging and NIRSpec multi object spectroscopy were obtained in a Director’s Discretionary Time programme (PID 4446, P.I. B. Frye) in April and May 2023. The exposure times vary from ≈ 0.7 hours to 1.4 hours in eight filters in the short and long wavelength channels, and after calibration with the JWST pipeline¹ (Bushouse et al. 2025), were combined into mosaics following the approaches first described by Koekemoer et al. (2011), updated for JWST (see Frye et al. 2024, section 2 and Table 1 for additional details). In Fig. 1, we show the NIRCam color composite image of the central region of G165. In this work, we use the original PEARLS imaging data (i.e., epoch 1)

¹ <https://github.com/spacetelescope/jwst>

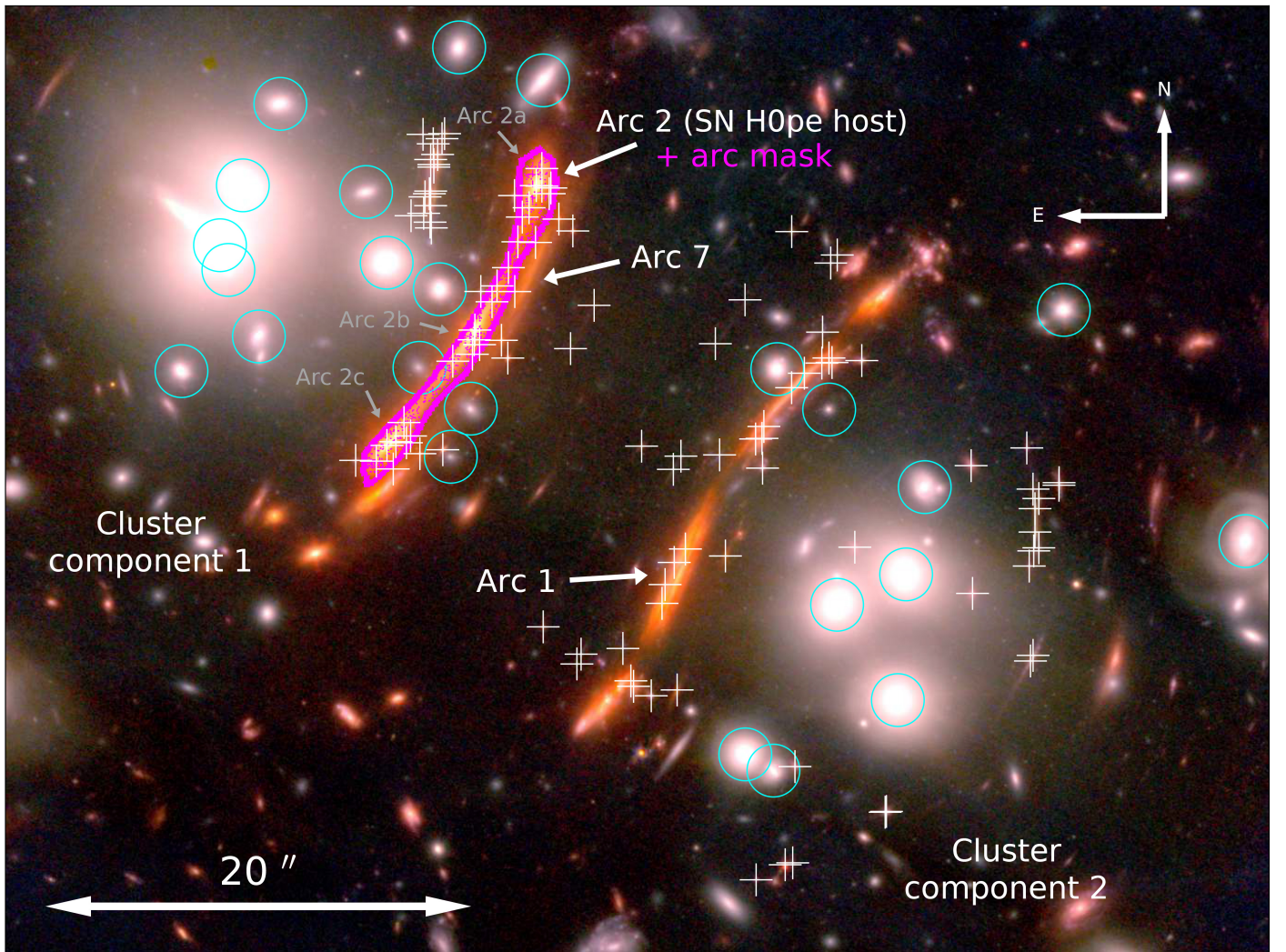


Fig. 1. JWST color composite image of G165 (where the combination for blue is F090W + F115W + F150W; green is F200W + F277W and red is F356W + F410M + F444W). White crosses indicate the position of point-like multiple images used as model constraints (presented in Frye et al. 2024). The magenta contour outlines the mask used to model the surface brightness of the SN H0pe host (Arc 2, composed of the SN host images 2a, 2b and 2c). Cyan circles show a subset of the cluster members included in our lens models. Our lens models also include two cluster-scale mass components, each located around the main concentrations of cluster members. The figure also indicates Arc 1 and Arc 7 which we mention in the text.

as these have longer exposure time than subsequent epochs², and the recently obtained template images without the SN were not available at the time of this analysis³. In particular, we use the same reduced data as in Pascale et al. (2025).

Spectroscopic redshift measurements were obtained with NIRSpec and additional ground based observations (for more details, see Frye et al. 2024), bringing the total number of families with measured spectroscopic redshifts to five. Regarding cluster members, 35 are spectroscopically confirmed in the redshift range $z = [0.329, 0.368]$, which corresponds to a peculiar velocity of 4000 km s^{-1} from the mean cluster redshift $z_d = 0.348$. This sample of cluster galaxies was used to determine the loci on the color-color space and select additional 130 cluster members by a photometric approach down to magnitude $m_{\text{F150W}} = 23.5$. Overall we consider the same 165 cluster members as used in all the lens models presented in Pascale et al. (2025). This catalog includes the 161 cluster members of Frye

et al. (2024) as well as 4 additional galaxies that either lack spectroscopic redshifts, are at a redshift close to the cluster's redshift, or are far from the cluster's centroid⁴.

3. Strong lens modeling of the galaxy cluster G165

3.1. Lens model with point-like image positions

To describe the lensing effect of G165 we assume two main mass components: one that represents the cluster-scale mass distribution and accounts mainly for the dark matter, and a second that describes the small scale galaxies that belong to the cluster. This merging cluster being clearly bimodal, is itself composed of two components. Since we are mainly interested in constraining our models at the location of the two main cluster components, we do not include an external shear or other larger scale components far outside the field of view of Fig. 1.

² Epochs 2 and 3 (PID 4446, P.I. B. Frye).

³ Epochs 4 and 5 (PID 4744, P.I.s B. Frye, J. Pierel). These template images will be presented in Agrawal, et al. 2025 (in prep.).

⁴ M. Pascale, private communication. Some details are also given in Pascale et al. (2025).

For the cluster-scale component, we adopt the pseudo-isothermal elliptical mass distributions (PIEMD; [Kassiola & Kovner 1993](#)), whose dimensionless projected mass distribution for a source at $z_s \rightarrow \infty$ is given by

$$\kappa(R) = \frac{\theta_E}{2 \sqrt{R(x, y, \varepsilon)^2 + r_{\text{core}}^2}}, \quad (1)$$

where θ_E is the Einstein radius (i.e. the mass normalization parameter) and r_{core} is the core radius. The quantity R is constant over ellipses with ellipticity ε , and is given by $R^2 = (x - x_c)^2/(1 + \varepsilon)^2 + (y - y_c)^2/(1 - \varepsilon)^2$, where x and y are along the semi-major and semi-minor axes, and (x_c, y_c) is the centroid of the profile. The profile is then rotated by a position angle ϕ . Our position angles are measured counterclockwise from the positive x axis. Therefore, the PIEMD mass profile is fully described by six parameters. The initial position of the two PIEMD profiles is located around the two main clumps of galaxy members (see Fig. 1).

In addition to the smooth cluster mass component, we account for the mass distribution of individual galaxies, some of these being indicated as cyan circles in Fig. 1. These galaxies mainly belong to the 161 of selected cluster members of G165 at redshift $z = 0.348$. We also place the 4 additional galaxies present in the catalog of [Pascale et al. \(2025\)](#) at the same redshift, given the current uncertainties regarding their nature (we defer testing this effect of this assumption to future models). Each galaxy in our model is parameterized by a circular dual pseudo iso-thermal mass density (dPIE, see [Elíasdóttir et al. 2007; Suyu & Halkola 2010](#)), with convergence given by

$$\kappa_i(R) = \frac{\theta_{E,i}}{2} \left(\frac{1}{R(x, y, \varepsilon)} - \frac{1}{\sqrt{R(x, y, \varepsilon)^2 - r_{\text{cut},i}^2}} \right), \quad (2)$$

where $r_{\text{cut},i}$ is the cut radius of cluster member i and R is the radial coordinate (with elliptical coordinates defined as in Eq. 1). As there are not enough constraints to optimize the parameters of all cluster members individually, we reduce the total number of free parameters by making use of the information from the light distribution of the cluster members. In particular, we fix the centroid of each galaxy to its observed light. We further reduce the number of parameters by assuming scaling relations similar to the Faber–Jackson relation for elliptical galaxies (e.g., [Jullo et al. 2007; Grillo et al. 2016](#)):

$$\theta_{E,i} = \theta_{E,\text{ref}} \left(\frac{L_i}{L_\star} \right)^{0.5}, \quad r_{\text{cut},i} = r_{\text{cut},\text{ref}} \left(\frac{L_i}{L_\star} \right)^{0.5}. \quad (3)$$

In particular, the relationship $\theta_{E,i} \propto L_i^{0.5}$ is obtained by assuming a constant mass-to-light ratio in cluster members. Our reference galaxy, which has $\theta_E = \theta_{E,\text{ref}}$ and $r_{\text{cut}} = r_{\text{cut},\text{ref}}$, is a bright cluster member of G165 located at (R.A., Dec.) = (11:27:06.6969, +42:27:50.375), which is outside the field of view of Fig. 1 (towards the West).

We use as lensing constraints 41 image families leading to 106 point-like images. A subset of 15 image families do not have spectroscopic redshifts, thus we leave their redshift free to vary (with uniform priors between 1 and 10). We note that 8 out of the 106 multiple images are located in the SN H0pe arc.

Our model contains 165 cluster members linked through the 2 parameters of Eq. 3 ($\theta_{E,\text{ref}}$ and $r_{\text{cut},\text{ref}}$) in addition to the two cluster-scale components with 6 parameters each, resulting in a total of $N_{\text{free}}^{\text{mass}} = 2 + 2 \times 6 = 14$ free mass model parameters. We

have 41 image families, which leads to $N_{\text{free}}^{\text{src-pt}} = 2 \times 41 + 15 = 97$ free source parameters (each source having two coordinates). We use 106 observed point-like positions so we have $N_{\text{con}}^{\text{img}} = 2 \times 106 = 212$ constraints. Therefore, our position-based lens model has $N_{\text{dof}}^{\text{pos}} = N_{\text{con}}^{\text{img}} - (N_{\text{free}}^{\text{mass}} + N_{\text{free}}^{\text{src-pt}}) = 101$ degrees of freedom.

3.2. Lens model with point-like and spatially-extended images of the SN host galaxy

Building upon our previous model, we now incorporate the full surface brightness distributions of the SN host galaxy (Arc 2), as constraint in addition to the majority of the point-like constraints used in Sect. 3.1. More specifically, we directly use the intensity values of the pixels of the lensed SN host galaxy as constraints. We thus remove the 8 point-like image families located within our arc mask (indicated with a magenta contour in Fig. 1), ending up with 84 instead of 106 point-like constraints in this extended-image lens model⁵. With this approach, we reduce the model uncertainties because of the additional constraints from the light distribution of Arc 2, and at the same time, reconstruct the morphology of the host galaxy of SN H0pe.

We use the software GLEE ([Suyu & Halkola 2010; Suyu et al. 2012](#)) because of its capability to model extended images of gravitational arcs, not only in galaxy-scale systems (e.g., [Suyu et al. 2013; Wong et al. 2017; Ertl et al. 2023](#)) but also on group and cluster scales (e.g., [Wang et al. 2022; Bolamperti et al. 2023; Acebron et al. 2024](#)). The mass modeling method using spatially extended images of lensed galaxies is described in [Suyu & Halkola \(2010\)](#), and here we summarize its main aspects.

We use the same parameterizations for the lens mass distribution (smooth cluster halo and the individual cluster galaxies) as described in the previous section. For a given set of values for these parameters, we can compute the deflection angle at each image pixel. Given the lensing deflection field, using the pixels in the arc mask, their associated error and a model of the point spread function (PSF), we can obtain the optimal reconstruction of the SN host galaxy on a regular grid of pixels on the source plane of the SN through a linear matrix inversion that is described in detail in [Suyu et al. \(2006\)](#). To construct the PSF model, we use three stars in the field and follow the same procedure described in [Ertl et al. \(2023\)](#). Our per-pixel error map is the quadratic sum of contributions from Poisson noise and background noise, which were obtained from the science data and the inverse variance weight maps, respectively. We use curvature regularization for inverting the pixelated source, which reduces the curvature (second derivatives) in the source intensity grid in order to avoid overfitting the noise in the data. This source intensity distribution is then mapped to the image plane using the deflection field and the PSF model, in order to obtain the reconstructed lensing arc that is then compared directly to the observed intensity pixel values inside the arc mask. Based on the difference between the reconstructed and observed arcs, we compute the likelihood of the extended image of Arc 2.

We use the filter F200W to perform our modeling of Arc 2 since it has the best compromise between signal-to-noise ratio (S/N) of the extended arc and JWST point spread function size. As the SN extent is not resolved, our extended source model should not attempt to reconstruct their flux on the source plane. We therefore boost the data uncertainties by a large factor ($\sim 10^3$) within circular regions of 4 pixels in radius centered on each SN image, which effectively exclude the corresponding pixels

⁵ Upon acceptance of the manuscript, we will release the full catalog of cluster members and lensing constraints used in our lens models.

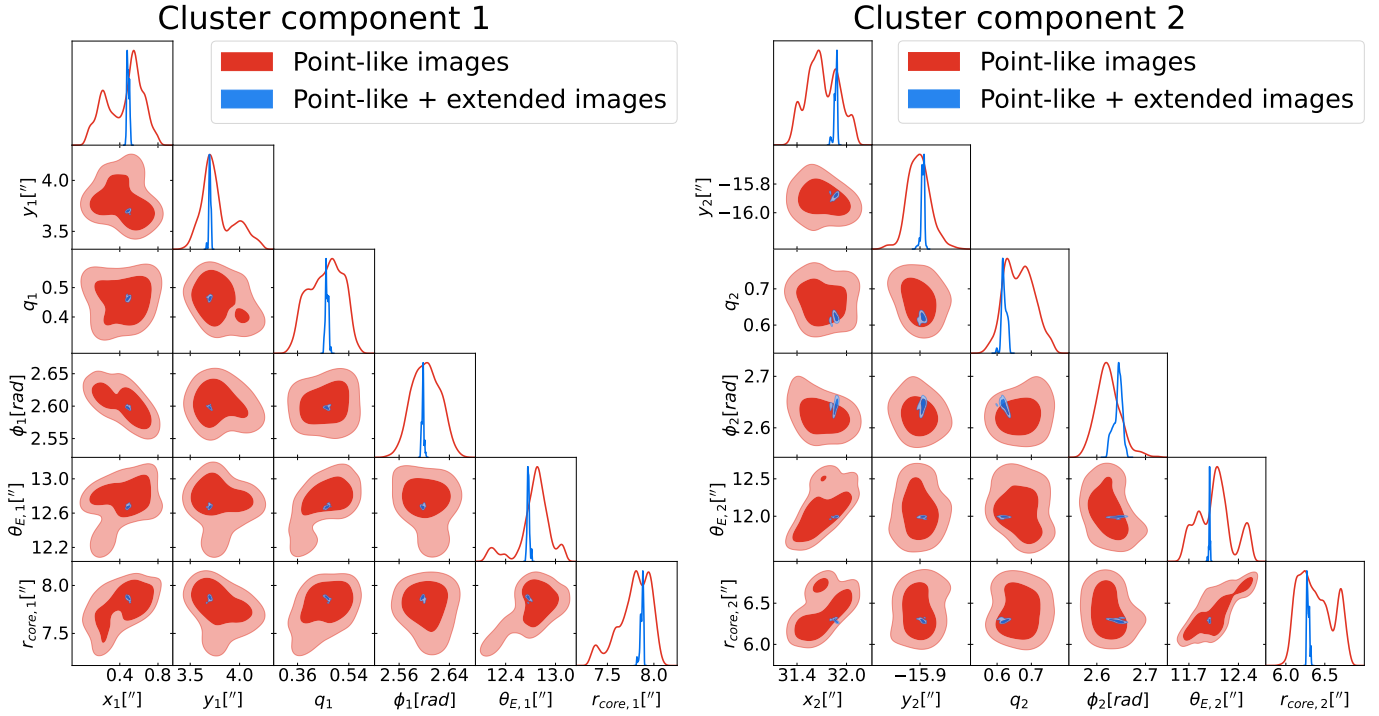


Fig. 2. Joint posterior distribution of the mass parameters for the two cluster-scale components. Contours are the 68% and 95% confidence levels for the model using only the point-like images as constraints (red) and the one including the full surface brightness of SN H0pe host galaxy (blue).

from the data likelihood term. Compared to our position-based model of Sect. 3.1, our extended-image model contains both additional parameters and constraints. The number of additional free parameters in this model is equal to the effective number of source pixels, which in our case is $N_{\text{free}}^{\text{src-ext}} \approx 135$ (for details of its computation, see Suyu et al. 2006). These pixels are constrained by the $N_{\text{con}}^{\text{arc}} = 29\,469$ pixels within the arc mask (shown in magenta in Fig. 1). Due to the removal of some image families within the arc, the updated number of point-like constraints is $N_{\text{con}}^{\text{img}} = 2 \times 84 = 168$ and number of free point-like source parameters is $N_{\text{free}}^{\text{src-pt}} = 2 \times 33 + 15 = 81$. Therefore, our complete lens model has $N_{\text{dof}}^{\text{pos+ext}} = (N_{\text{con}}^{\text{img}} + N_{\text{con}}^{\text{arc}}) - (N_{\text{free}}^{\text{src-pt}} + N_{\text{free}}^{\text{src-ext}}) = 29\,421$ degrees of freedom.

We note that the tens of thousands of arc pixels overpower the few hundreds of point-like images available. The position-based likelihood term thus becomes subdominant compared to the extended-image likelihood term when evaluated close to the best-fit solution. Since here we focus on the impact of modeling the extended surface of the SN H0pe host, we do not attempt to re-weight the two likelihoods so the extended-image term remains naturally dominant. We note however that Schuldt et al. (in prep.) explores different likelihood weighting choices, finding significant improvements in mass model uncertainties in all cases.

We run MCMC chains to sample the lens mass parameters using the extended image likelihood. We check convergence using the power-spectrum method of Dunkley et al. (2005). The resulting mass parameter constraints are shown in Fig. 2 by the blue contours, which are substantially tighter compared to the image position constraints (red contours) from Sect. 3.1. Averaging over all mass model parameters—halo components and cluster members—we find that the posterior uncertainty is reduced by a factor of ≈ 12 . This is comparable to the gain quoted Schuldt et al. (in prep.) after including extended image mod-

eling of the SN Refsdal host in their lens model of the cluster MACS J1149.5+2223.

3.3. Other extended arcs and lens model flexibility

We performed the extended-image modeling of the SN H0pe host (Arc 2), but did not reconstruct other arcs visible in Fig. 1 for two reasons: (1) our work focuses primarily on the host of SN H0pe and (2) the computational costs would significantly increase. However, given the bimodality and configuration of the cluster G165, Arc 2 appears closer to the cluster component 1. Hence, one may expect the parameters of that component to be better constrained, compared to those of component 2. Splitting the average gain over the mass parameters of components 1 and 2 lead to ≈ 13 and ≈ 11 factors of improvement, respectively. Arc 2 provides therefore slightly more constraints on the cluster component 1. Modeling the extended surface brightness of the arcs appearing closer to the cluster component 2 will further reduce the uncertainty on all mass model parameters, even at the position of the lensed SN images. Nevertheless, it is not clear if the uncertainty gain would be valuable for the purpose of time-delay cosmography, given other sources of systematic errors and possible limitations of the mass model, as discussed below.

Our extended image modeling reveals residuals along the reconstructed Arc 2 (see Appendix B for more details). Part of these residuals (typically on the scale of a few pixels) could be attributed to specificity of the source reconstruction technique. However, residuals on the scale of the multiple images—which are more prominent than the small-scale residuals—could be instead the sign of missing flexibility in the lens model. Without adding any additional component to the model, we could for instance relax the scaling relation employed to scale the mass parameters of cluster members (Eq. 3) for galaxies in the vicinity of the modeled arc. For these galaxies, additional measurements of the stellar velocity dispersion of these galaxies could comple-

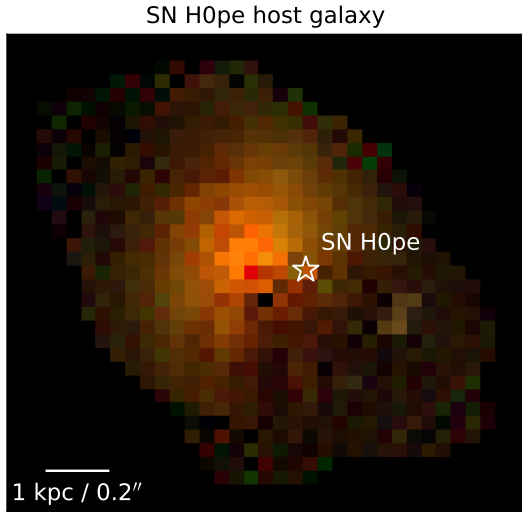


Fig. 3. Color composite of the reconstructed source-plane image of the SN H0pe host galaxy ($z = 1.78$). The filters F090W, F150W and F200W correspond to the blue, green and red channels, respectively. The white star indicates the position of SN H0pe. The pixel scale is $0.048''$.

ment the lensing constraints. Alternatively extra degrees of freedom could also be introduced in the cluster-scale components, such as multipoles or a variable density slope. Such improvements to the extended-image lens model are deferred to a future work.

4. SN H0pe host galaxy

4.1. Surface brightness reconstruction

Our extended model of the SN H0pe host was used in Pierel et al. (2024) to obtain the photometry of the SN images and measure the photometric time delays used as constraints in Pascale et al. (2025) for inferring H_0 . In more detail, our Arc 2 model was used to subtract off the flux of the host at each SN image position. While we used only the F200W data to constrain the mass model parameters, we used the best-fit lens model to reconstruct the extended source in other bands, which allowed Pierel et al. (2024) to infer the photometry in all filters bluer than F356W. Figure 3 of their paper shows the SN images after subtraction of our multi-band arc model, and we refer the interested reader to their paper for more details.

In Appendix B we show the complete set of source models. In the filter used for our lens model (F200W) and also redder filters, we notice residuals in high S/N areas in two out of the three lensed images of the SN host galaxy (middle and bottom ones in the arc). More specifically, the middle image of the SN host produces positive residuals, meaning our model is under-magnifying the host, while it is the opposite behavior for the bottom image. The top image is however significantly better reproduced by our lens model. Such residuals may indicate that the two cluster-scale PIEMD components, especially the one located to the east of Arc 2, are not accurately representing the deflection field across the entire arc. Additionally, intra-cluster light (ICL) and possibly light from low surface brightness cluster members or lower-redshift galaxy interlopers that fall below the detection limit can also explain the excess light in the vicinity of Arc 2b (see e.g., Pascale et al. 2022). Including the surface brightness model of foreground objects is deferred to a future work (Galan et al., in prep.).

We also construct the color image of the SN host shown in Fig. 3. Despite the low S/N in bluer filters (especially F090W), we see a clear color gradient: the core of the SN H0pe host galaxy appears redder than its outskirts. As shown in Fig. 3, SN H0pe lies about 1 kpc away from its host centroid, in a region that appears slightly darker than other regions at similar galactocentric radii. Source regions that appear darker may be attenuated by dust, which we investigate next.

4.2. Dust extinction in the image plane

Dust lanes are visible in the SN host images, typically in the bluer filters of the set (e.g., notice the redder regions in Fig. 1 of Pascale et al. 2025). The presence of dust can affect photometric measurements, in particular the observed brightness of the SN images, which may in turn bias the time delays used in cosmographic analyses. Recent works using JWST data inferred some dust properties of the SN H0pe host: Frye et al. (2024) measured quantities such as the color excess $E(B - V)$ via a NIRCam+NIRSpec spectrophotometric analysis, Chen et al. (2024) fitted NIRSpec spectra at the position of each image to infer the extinction ratio $R(V)$ in addition to $E(V - B)$, while Pierel et al. (2024) constrained the total dust extinction in the V-band $A_V \equiv R(V) \times E(B - V)$ jointly with $R(V)$ and the time delays. Complementary to these approaches, we build here the dust extinction map of the SN H0pe host, by mapping the spatial distribution of A_V across the entire Arc 2.

We follow the procedure described in Suyu et al. (2009, in particular their Sect. 5.4) to build a dust extinction map from the NIRCam images. We first express the observed magnitude $m_{F,\text{observed}}$ in a given filter F in terms of A_V and the intrinsic magnitude of the reddest wavelength band $m_{1,\text{intrinsic}}$ as

$$m_F \equiv m_{F,\text{observed}} = m_{1,\text{intrinsic}} + Q_F + A_V k_F + n_F, \quad (4)$$

where $k_F \equiv A_F/A_V$ are constants given by the extinction law and n_F is the noise in the data of wavelength band F . We also defined Q_F as the intrinsic color with respect to the reddest filter:

$$Q_F = m_{F,\text{intrinsic}} - m_{1,\text{intrinsic}}, \quad (5)$$

where $F = 1, \dots, N_b$ is the sequence of N_b filters ordered from the reddest to the bluest one (note that by construction $Q_1 = 0$). We convert the original flux data units (MJy/st) to AB magnitudes using zero-point values of 28.0874 (blue arm) and 28.0863 (red arm)⁶.

Suyu et al. (2009) showed that A_V and $m_{1,\text{intrinsic}}$ can be jointly solved for. Here we are interested in A_V , which has the following analytical solution:

$$A_V = \left[\frac{1}{N_b} \left(\sum_F k_F \right) \left(\sum_F m_F \right) - \frac{1}{N_b} \left(\sum_F k_F \right) \left(\sum_F Q_F \right) - \left(\sum_F k_F m_F + \sum_F k_F Q_F \right) \right] / \left[\frac{1}{N_b} \left(\sum_F k_F \right)^2 - \sum_F k_F^2 \right], \quad (6)$$

⁶ This is slightly different from the zero-point value given in Windhorst et al. (2023, that is 28.0865), which we attribute to the slightly different reduction of Frye et al. (2024) who used calibration files available to them at that time.

To compute A_V we need to estimate the intrinsic colors Q_F from Eq. 5. We use filters F200W, F270W, F356W and F444W, the last of which is the reddest and thus our reference filter (i.e., with $F = 1$). We do not use any of the NIRCam filters bluer than F200W since the arc S/N is too faint, and the noisy patterns introduce artifacts in the dust extinction map (see Fig. B.1). Since bluer filters have intrinsically a better resolution than redder ones, we first re-convolve all filters such that they match the resolution of our reference one. We construct resolution-matching PSF kernels using the `create_matching_kernel()` routine (using a `CosineBellWindow` regularizing function to avoid artifacts) from the `PHOTUTILS` Python package (Bradley et al. 2024). In this process, we found that PSF models created with `STARRED` (Michalewicz et al. 2023; Millon et al. 2024)—instead of the stacked-stars models used for lens modeling—improved both the resolution-matching step and the final dust extinction map results⁷.

We then visually identify a region in the arc that is likely not affected by dust (indicated in the left of Fig. 4). Within this region, we then carefully select a smaller region that has the bluest color with respect to F444W. We restrict the region in two steps. We first apply a 5σ noise threshold simultaneously for both filters for a given pair (Eq. 5). We then consider as our final color estimate the first percentile value of the resulting distribution, namely the pixel that is bluer than 99% of the pixels within the restricted region. This procedure ensures that we are excluding pixels that are not representative of the bulk distribution of colors across our region. Such outlier pixels may appear too blue due to noise fluctuations or localized bright features such as star forming regions (these could be located either in the foreground or in the host galaxy).

Having estimated the intrinsic colors Q_F , we evaluate Eq. 6 for every pixel of the arc, assuming the reddening law from Fitzpatrick (1999)⁸ and extinction ratio $R_V = 3.1$ (i.e., galactic extinction), again following Suyu et al. (2009). We note that $\lesssim 10\%$ pixels obtain slightly negative A_V values, which is not physical. Nevertheless, these values are limited to pixels close to the edge of the arc mask, which contain flux from the ICL or galaxies other than the SN H0pe host, have low S/N or have negative flux due to a slight over-subtraction of the background level. We show in Fig. 4 the map of dust extinction A_V for each pixel within the arc mask, excluding pixels around the SN images. The middle and right panels of Fig. 4 show that, as expected, areas with larger dust extinction align well with lower-intensity regions of the arc in bluer filters (for example in F200W, but it is also clear in F150W despite lower S/N).

We have built the A_V map excluding circular regions centered on each of the SN images⁹. However, we can estimate the dust extinction at the position of SN H0pe by interpolating of the A_V values within the masked regions. We use nearest-neighbor interpolation, since this is based on minimal assumptions regarding the underlying A_V spatial variations, and is accurate enough for the few pixels we are interpolating over. Although in theory, the dust extinction at the position of each SN image should be identical, it is not due to various reasons such as data noise, PSF model (original and resolution-matching kernels) and light contamination from foreground objects. Therefore, we consider the

⁷ The lens modeling results described in Sect. 3.2 are not significantly impacted when using the alternative PSF models.

⁸ We note that using the extinction law of Cardelli et al. (1989) instead does not change our results. We use the Python package `extinction` for its implementation of various extinction laws.

⁹ These regions are identical to those excluded from the extended source model likelihood, as described in Sect. 3.2.

mean over the three images as our fiducial value, for which we find $A_V^{\text{H0pe}} = 0.94 \pm 0.25$. The quoted uncertainty is a quadratic sum of three error terms. For the statistical error term, we emulate 100 realizations of the data and consider the resulting standard deviation of A_V , averaged over the three SN image positions. We then estimate a systematic error term due to the choice of the PSF model, by considering the mean difference between the A_V^{H0pe} values obtained with the PSF models used in lens modeling and those obtained using `STARRED`. Our last error term is the standard deviation over the A_V values interpolated at each position of the SN images (we use Bessel correction for the standard deviation due to the small sample size). These three error terms due to data noise, PSF model and image position amount to 1%, 6% and 93% of the total variance, respectively.

4.3. Dust extinction in the source plane

We use the dust extinction map shown in Fig. 4 and reconstruct it on the source plane using our lens model from Sect. 3.2. As the `GLEE` source reconstruction algorithm requires an estimate of the uncertainty per pixel, we approximate it by $\sqrt{A_V}$ (i.e., similar to a shot noise estimate), which results in a reasonable source-plane reconstruction. We show the source-plane dust extinction map of the SN H0pe host galaxy in the top panel of Fig. 5. SN H0pe is located on the outskirt of a large region with significant dust extinction with $A_V \gtrsim 1$. We do not quote an interpolated A_V^{H0pe} value from our source-plane dust extinction map. Such an estimate would be too uncertain due the imperfect PSF model (whose effect is more pronounced than in the image plane), pixelation effects of the source reconstruction, as well as the specific choice for the A_V per-pixel uncertainty. Instead, our image-plane estimate detailed in Sect. 4.2 is more robust, and should thus be preferred.

We find the dust distribution in the SN host to be strongly asymmetric. While early-type galaxies and mid-type spirals generally display symmetric and radially decreasing A_V profiles (see e.g., Kim et al. 2019), the host of SN H0pe clearly has stronger reddening southward of the galaxy center. Such dust distribution could be explained by outflow mechanisms that triggered a burst of star formation. Inflow of dusty material could alternatively explain the asymmetric feature visible in the dust extinction map. Dedicated analyses of the available NIRSpec spectra from each lensed image could perhaps give us insights, although additional observations at sub-mm wavelengths would more certainly help to know the origin of the asymmetric dust distribution.

We also note a relatively high-extinction region at the bottom of the source plane grid visible in Fig. 5; this region maps to the edge of the arc mask in the bottom lensed image (see right panel of Fig. 4) and is mainly caused by low S/N in the bluer filters, as well as possible contamination from the neighboring arc (see Sect. 4.5). To assess if this is high-extinction region has high uncertainty, we consider the A_V standard deviation in each pixel of the source plane from 100 random lens model posterior samples. The resulting uncertainty map is shown in the bottom of Fig. 5. From this map we see that the bottommost high-extinction region is not particularly uncertain based on our lens model, and is likely a real feature from the image-plane dust distribution. We do not build a complete uncertainty map that include other sources of errors, since these are harder to properly propagate to the source plane.

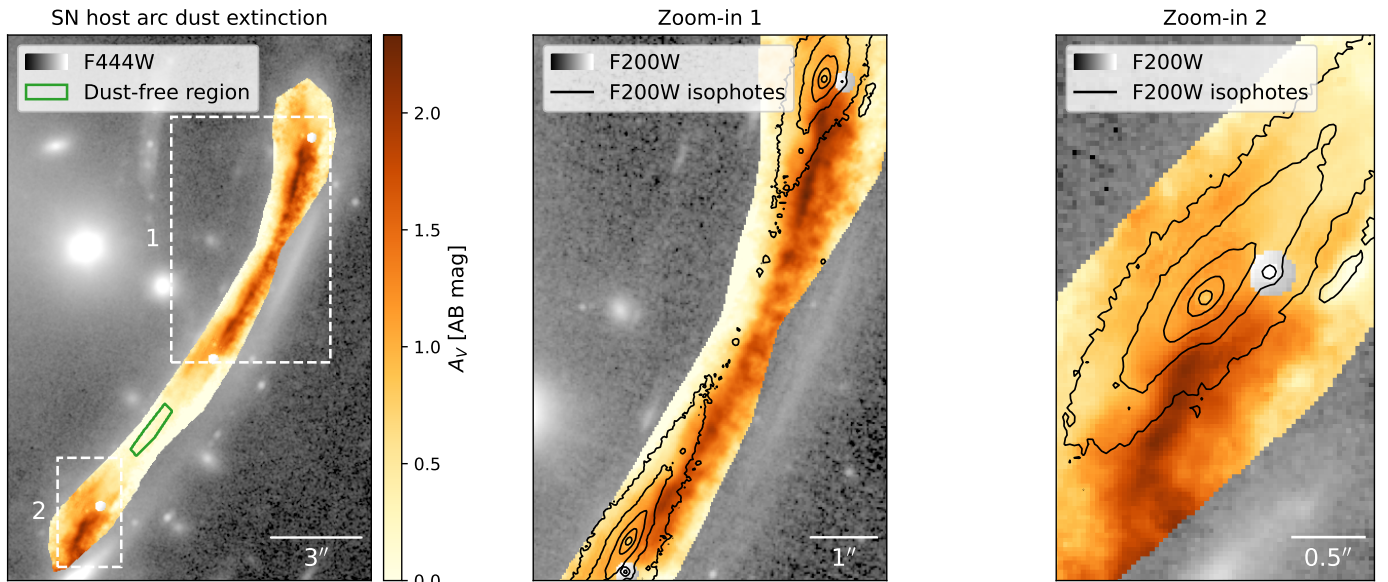


Fig. 4. Image-plane dust extinction map of SN H0pe host galaxy. Left panel: dust extinction map within the arc mask and at the resolution of the F444W data, which is also shown in grayscale (see Sect. 4.2 for more details). The dashed line rectangles indicate the zoom-in regions of the middle and right panels. These panels show the F200W data in grayscale and corresponding isophotes (logarithmically spaced), showing consistency between the dust extinction and dimmer regions of the arc. In all panels, North is at the top and east is to the left..

4.4. Comparison with previous work and influence on H_0

Pierel et al. (2024) inferred the dust extinction at the position of the SN H0pe as a by-product of their photometric time delay measurement. They performed spectral energy distribution (SED) fitting with free parameters that include R_V and A_V at the position of SN H0pe and inferred $A_V^{\text{H0pe,P24}} = 1.21 \pm 0.11$. This is in relatively good agreement with our measurement, at the $\sim 1\sigma$ level. This is noteworthy because these two measurements are independent, using in part the same data but in different ways. Pierel et al. (2024) performed PSF photometry on the host-subtracted images based on our extended host model from Sect. 3.2, using only the pixels within small regions around each SN image. In contrast, we excluded these same regions to build our dust extinction map and estimated A_V^{H0pe} through interpolation. Despite the different approaches, they are complementary and we arrive at similar dust extinction values.

Chen et al. (2024) also inferred dust parameters jointly with the spectroscopic time delays of SN H0pe. They fitted the NIR-Spec spectra of each image with a set of shared parameters, in particular R_V and $E(B - V)$. They inferred $R(V) = 2.7^{+0.2}_{-0.1}$ and $E(B - V) = 0.27 \pm 0.01$, which leads to a total extinction of $A_V^{\text{H0pe,C24}} = 0.73^{+0.08}_{-0.05}$. While their result is unsurprisingly more precise than ours (since they use high-resolution spectrum fitting), both results are in good agreement at the $\sim 0.8\sigma$ level. Here again, it is reassuring that very different approaches, either based on NIRCam photometry only or NIRSpec spectroscopy only, lead to consistent measurements. More recently, Grayling et al. (2025) remeasured the time delays between the SN H0pe images by performing the SED modeling of the photometric light curves from Pierel et al. (2024) and include the effect of microlensing in their model. In addition to the SN time of maximum, they measured $A_V^{\text{H0pe,G25}} = 0.95 \pm 0.14$. We find again excellent agreement with our measurements.

Although not precisely at the position of SN H0pe, Frye et al. (2024) measured the color excess $E(B - V)$ for Arcs 2a and 2c via NIRCam+NIRSpec spectrophotometric SED fitting. The NIR-

Spec spectra extracted by Frye et al. (2024) do not contain the images of SN H0pe, but rather regions close the center of the host galaxy (see the top panel of their Fig. 4). For these regions, they measured $E(B - V) = 0.22 \pm 0.04$ and $E(B - V) = 0.20 \pm 0.04$ for Arcs 2a and 2c, respectively. Assuming $R(V) = 3.1$ (i.e., what we assume in Sect. 4.2), their measurements translate to $A_V^{\text{2a,F24}} = 0.68 \pm 0.1$ and $A_V^{\text{2c,F24}} = 0.62 \pm 0.1$. One can read $A_V \lesssim 1$ within the central isophote of our source-plane dust extinction map in Fig. 5 (top panel), so both results broadly agree with each other.

The photometric time delays of SN H0pe measured in Pierel et al. (2024) using our extended arc model were then used in Pascale et al. (2025) for cosmography. Therefore, we can—at least qualitatively—discuss the influence of the dust extinction on the inferred value of H_0 . Based on the joint posterior distributions shown in Fig. 5 of Pierel et al. (2024) we note mild correlations between the two time delays and A_V , slightly more pronounced for Δt_{ba} between images 2a and 2b of SN H0pe (top and middle images, see Fig. 1). More specifically, A_V and Δt_{ba} are anti-correlated. Our lower value of A_V^{H0pe} compared to the best-fit of Pierel et al. (2024) would decrease the time delay Δt_{ba} by ~ 20 days. Qualitatively, a lower time delay will lead to a larger H_0 value (this can also be deduced from Fig. 3 of Pascale et al. 2025). Better quantification of the real impact on H_0 is non-trivial since the final measurement of Pascale et al. (2025) is the result of a thorough Bayesian analysis to properly combine many underlying models. We note however that dust extinction may influence the results of time-delay cosmography analyses with the SN H0pe.

4.5. Intrinsic colors of Arc 2 and dust in Arc 7

As detailed in Sect. 4.2, our dust extinction procedure uses an estimation of the SN host intrinsic colors. We have carefully selected a specific region in Arc 2 which is likely unaffected by dust, and assumed it is representative of the intrinsic color of the SN host galaxy. While this assumption holds for a symmetric

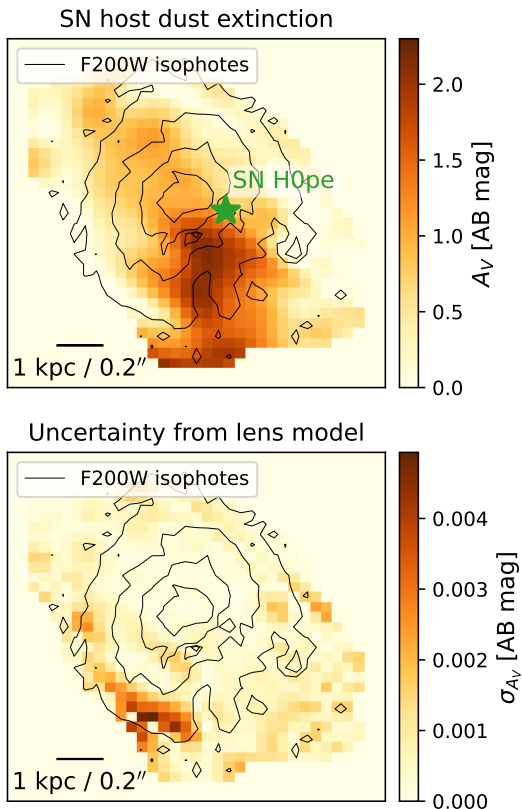


Fig. 5. Top panel: Dust extinction map of SN H0pe host galaxy, reconstructed in the source plane based on our extended-image lens model. The green star shows the position of the SN with respect to its host, whose (logarithmically spaced) isophotes are indicated with thin black contours. We note the consistency between the perturbed isophotes and the dust extinction map. The bottommost high-extinction feature (~ 3 bottom rows of the source-plane grid) is mainly due to low data S/N and image-plane flux contamination at the edge of the arc mask. North is at the top and east is to the left. Bottom panel: A_V uncertainty due to the posterior uncertainty of our strong lensing model. In both panels, the pixel scale is $0''.048$.

and smooth galaxy such as an elliptical, it may not be accurate for one with a more complex morphology. Smooth variations of the intrinsic color may also be caused by local changes in stellar metallicities and stellar populations. The joint NIRCam and NIRSpec analysis of two of the three images of the host, presented in detail by Frye et al. (2024), indicates that it is a moderately dusty and massive star-forming galaxy, with a possibly complex star formation history. Our dust extinction map corroborates such conclusions. The low S/N in bluer filters as well as the light contamination from nearby arcs—including galaxies with very similar colors, belonging to the same $z = 1.78$ group as the SN host (Frye et al. 2024)—make it challenging to obtain better estimates of the intrinsic colors. The estimation presented here carefully excluded regions that were either too low S/N or whose colors could be affected by local features (e.g., SN images, compact star-forming regions, etc.). An alternative approach to ours would be to perform SED fitting for each pixel within the arc mask. Such an approach would remove the need to assume intrinsic colors that do not vary over the scale of the galaxy. However, in addition to be computationally more expensive, per-pixel SED fitting would perhaps be limited by the relatively low number of JWST bands available, due to known de-

generacies between the dust extinction, stellar populations and metallicity.

We note that the SN H0pe host galaxy (Arc 2) appears very close to another equally extended arc (referred to as Arc 7 and indicated in Fig. 1). From lensing geometry, one can argue that Arc 7 corresponds to a larger Einstein radius than Arc 2, hence further away from us. However, other arguments using symmetry points within each arc could be in favor of the opposite situation. If Arc 7 is indeed closer to us and contains a significant amount of dust, then it could be responsible for at least some of the dimming and reddening visible along Arc 2. To the best of our knowledge, there is currently no spectroscopic redshift for Arc 7. Frye et al. (2019) estimated $z = 1.7$ from their lens models, and Pascale et al. (2022) found a photometric redshift of $z = 1.86^{+0.29}_{-0.28}$. In all our models, the redshift of Arc 7 is left as a free parameters but given the low number of secure point-like constraints associated to it (3), this redshift is not robustly constrained. Therefore, one cannot currently rule out the possibility that Arc 7 contributes to the observed dust extinction. We emphasize that our image-plane dust extinction map (Fig. 4) are unaffected by the true distance of Arc 7 relative to Arc 2, since we do not make any assumption regarding the origin of the dust. On the contrary, our source-plane dust extinction map (top panel of Fig. 5) could be modified by the knowledge of the redshift of Arc 7. For instance, the southernmost area with significant A_V values in our source-plane extinction may be the result of dust from another lensed galaxy, which could be Arc 7 if it is located in the foreground.

5. Conclusions

The full exploitation of strongly lensed Type Ia SNe like SN H0pe relies on a good lens model. In this work, we have shown a significant precision gain in mass models parameters after incorporating all the pixels from the arc hosting SN H0pe. We have performed two lens models of the host cluster G165: one following the traditional position-based approach, namely using point-like multiple images as constraints, followed by an improved model that jointly reconstructs the full surface brightness of the arc. We find that including the extended SN host as constraints decreases the uncertainty on mass model parameters by a factor of $\gtrsim 10$. This gain precision would translate to a gain on the precision of the Hubble constant, which would need to be quantified by following the approach of Pascale et al. (2025).

Our improved lens model, the first that also reconstructs the surface brightness of the SN H0pe host galaxy, allowed us to study the dust distribution in this galaxy. In particular, we computed the dust extinction map over the entire gravitational arc, leveraging the color information the JWST/NIRCam dataset. We find good agreement between the visibly attenuated regions in the arc and the regions with high values of extinction coefficient. Our lens model allowed us to map the dust extinction back to the plane of the host galaxy, showing that SN H0pe lies on the edge of a dust region. The relatively complex but moderate dust extinction over the host is qualitatively consistent with the conclusions of Frye et al. (2024) based on simultaneous fitting of the JWST/NIRCam imaging and JWST/NIRSpec spectroscopy of the arc. Our dust extinction map allowed us to estimate a V-band extinction of $A_V^{\text{H0pe}} = 0.94 \pm 0.25$ at the position of SN H0pe. Our estimate is in good statistical agreement with the fully independent value of Pierel et al. (2024) based on multi-epoch photometry and of Chen et al. (2024) based on the multi-epoch spectroscopy.

Our direct modeling of the SN host surface brightness revealed model residuals along the arc that point towards limitations of the parametric model of G165. In a follow-up work (Galan et al., in prep.), we will improve upon our lens models by including foreground light from the brightest cluster members and ICL, and by increasing the flexibility of both the lens and source models to better fit the observations. We will use the approach introduced in Galan et al. (2024) using the lens modeling code HERCULENS (Galan et al. 2022). Comparing our present and future lens models with those used in Pascale et al. (2025) will enable further investigation of the systematic biases reported in Agrawal et al. (2025), ultimately improving the measurement of H_0 with time-delay cosmography on cluster scales. Moreover, newly obtained JWST/NIRCam template images will, together with our results on the spatially-resolved dust extinction, enable improved photometry and time delays from SN H0pe.

Acknowledgements. SS has received funding from the European Union's Horizon 2022 research and innovation programme under the Marie Skłodowska-Curie grant agreement No 101105167 — FASTIDIOUS. SHS and SE thank the Max Planck Society for support through the Max Planck Fellowship for SHS. This project has received funding from the European Research Council (ERC) under the European Union's Horizon 2020 research and innovation programme (LENSNOVA: grant agreement No 771776). This work is supported in part by the Deutsche Forschungsgemeinschaft (DFG, German Research Foundation) under Germany's Excellence Strategy – EXC-2094 – 390783311. RAW acknowledges support from NASA JWST Interdisciplinary Scientist grants NAG5-12460, NNX14AN10G and 80NSSC18K0200 from GSFC. CG acknowledges financial support through grant MIUR2020 SKSTHZ. AA acknowledges financial support through the Beatriz Galindo programme and the project PID2022-138896NB-C51 (MCIU/AEI/MINECO/FEDER, UE), Ministerio de Ciencia, Investigación y Universidades. J.M.D. acknowledges the support of projects PID2022-138896NB-C51 (MCIU/AEI/MINECO/FEDER, UE) Ministerio de Ciencia, Investigación y Universidades and SA101P24 (Junta de Castilla y León). RAW acknowledges support from NASA JWST Interdisciplinary Scientist grants NAG5-12460, NNX14AN10G and 80NSSC18K0200 from GSFC. This research made use of SciPy (Virtanen et al. 2020), NumPy (Oliphant 2006; Van Der Walt et al. 2011), MATPLOTLIB (Hunter 2007), ASTROPY (Astropy Collaboration et al. 2013; Price-Whelan et al. 2018) and GETDIST (Lewis 2019).

References

Acebron, A., Grillo, C., Suyu, S. H., et al. 2024, ApJ, 976, 110
 Agrawal, A., Pierel, J. D. R., Narayan, G., et al. 2025, Testing Lens Models of PLCK G165.7+67.0 Using Lensed SN H0pe
 Astropy Collaboration, Robitaille, T. P., Tollerud, E. J., et al. 2013, A&A, 558, A33
 Bolamperti, A., Grillo, C., Cañameras, R., Suyu, S. H., & Christensen, L. 2023, A&A, 671, A60
 Bradley, L., Sipőcz, B., Robitaille, T., et al. 2024, astropy/photutils: 2.0.2
 Bushouse, H., Eisenhamer, J., Dencheva, N., et al. 2025, JWST Calibration Pipeline
 Cañameras, R., Nesvadba, N. P. H., Guery, D., et al. 2015, A&A, 581, A105
 Cañameras, R., Nesvadba, N. P. H., Limousin, M., et al. 2018, A&A, 620, A60
 Cardelli, J. A., Clayton, G. C., & Mathis, J. S. 1989, ApJ, 345, 245
 Chakraborty, S., Sadler, B., Hoeflich, P., et al. 2024, ApJ, 969, 80
 Chen, W., Kelly, P. L., Frye, B. L., et al. 2024, ApJ, 970, 102
 Ding, H., Shu, Y., Chen, Y., et al. 2025, Research in Astronomy and Astrophysics, 25, 065013
 Dunkley, J., Bucher, M., Ferreira, P. G., Moodley, K., & Skordis, C. 2005, MNRAS, 356, 925
 Elíasdóttir, Á., Limousin, M., Richard, J., et al. 2007, arXiv e-prints, arXiv:0710.5636
 Ertl, S., Schuldt, S., Suyu, S. H., et al. 2023, A&A, 672, A2
 Fitzpatrick, E. L. 1999, PASP, 111, 63
 Frye, B., Pascale, M., Cohen, S., et al. 2023, Transient Name Server AstroNote, 96, 1
 Frye, B. L., Pascale, M., Pierel, J., et al. 2024, ApJ, 961, 171
 Frye, B. L., Pascale, M., Qin, Y., et al. 2019, ApJ, 871, 51
 Galan, A., Caminha, G. B., Knollmüller, J., Roth, J., & Suyu, S. H. 2024, A&A, 689, A304
 Galan, A., Vernardos, G., Peel, A., Courbin, F., & Starck, J. L. 2022, A&A, 668, A155
 Grayling, M., Thorp, S., Mandel, K. S., et al. 2025, arXiv e-prints, arXiv:2510.11719
 Grillo, C., Karman, W., Suyu, S. H., et al. 2016, ApJ, 822, 78
 Hakobyan, A. A., Barkhudaryan, L. V., Karapetyan, A. G., et al. 2020, MNRAS, 499, 1424
 Harrington, K. C., Yun, M. S., Cybulska, R., et al. 2016, MNRAS, 458, 4383
 Hunter, J. D. 2007, Computing in Science & Engineering, 9, 90
 Jullo, E., Kneib, J. P., Limousin, M., et al. 2007, New Journal of Physics, 9, 447
 Kamienski, P. S., Frye, B. L., Windhorst, R. A., et al. 2024, ApJ, 973, 25
 Kassiola, A. & Kovner, I. 1993, ApJ, 417, 450
 Kelly, P. L., Hicken, M., Burke, D. L., Mandel, K. S., & Kirshner, R. P. 2010, ApJ, 715, 743
 Kelly, P. L., Rodney, S. A., Treu, T., et al. 2015, Science, 347, 1123
 Kim, D., Jansen, R. A., Windhorst, R. A., Cohen, S. H., & McCabe, T. J. 2019, ApJ, 884, 21
 Koekemoer, A. M., Faber, S. M., Ferguson, H. C., et al. 2011, ApJS, 197, 36
 Lewis, A. 2019, arXiv e-prints, arXiv:1910.13970
 Meldorf, C., Palmese, A., Brout, D., et al. 2023, MNRAS, 518, 1985
 Michalewicz, K., Millon, M., Dux, F., & Courbin, F. 2023, Journal of Open Source Software, 8, 5340
 Millon, M., Michalewicz, K., Dux, F., Courbin, F., & Marshall, P. J. 2024, AJ, 168, 55
 Oliphant, T. E. 2006, A guide to NumPy, Vol. 1 (Trelgol Publishing USA)
 Pascale, M., Frye, B. L., Dai, L., et al. 2022, ApJ, 932, 85
 Pascale, M., Frye, B. L., Pierel, J. D. R., et al. 2025, ApJ, 979, 13
 Perera, D., Jr, J. H. M., Williams, L. L. R., et al. 2025, The Open Journal of Astrophysics, 8, 37
 Pierel, J. D. R., Frye, B. L., Pascale, M., et al. 2024, ApJ, 967, 50
 Planck Collaboration, Aghanim, N., Altieri, B., et al. 2015, A&A, 582, A30
 Popovic, B., Wiseman, P., Sullivan, M., et al. 2024, MNRAS, 534, 2263
 Price-Whelan, A. M., Sipőcz, B. M., Günther, H. M., et al. 2018, AJ, 156, 123
 Roman, M., Hardin, D., Betoule, M., et al. 2018, A&A, 615, A68
 Ruiter, A. J. & Seitzenzahl, I. R. 2025, A&A Rev., 33, 1
 Sheu, W., Cikota, A., Huang, X., et al. 2024, ApJ, 973, 3
 Suyu, S. H., Auger, M. W., Hilbert, S., et al. 2013, ApJ, 766, 70
 Suyu, S. H. & Halkola, A. 2010, A&A, 524, A94
 Suyu, S. H., Hensel, S. W., McKean, J. P., et al. 2012, ApJ, 750, 10
 Suyu, S. H., Marshall, P. J., Blandford, R. D., et al. 2009, ApJ, 691, 277
 Suyu, S. H., Marshall, P. J., Hobson, M. P., & Blandford, R. D. 2006, MNRAS, 371, 983
 Uddin, S. A., Burns, C. R., Phillips, M. M., et al. 2020, ApJ, 901, 143
 Van Der Walt, S., Colbert, S. C., & Varoquaux, G. 2011, Computing in Science & Engineering, 13, 22
 Virtanen, P., Gommers, R., Oliphant, T. E., et al. 2020, Nature Methods, 17, 261
 Wang, H., Cañameras, R., Caminha, G. B., et al. 2022, A&A, 668, A162
 Windhorst, R. A., Cohen, S. H., Jansen, R. A., et al. 2023, AJ, 165, 13
 Wong, K. C., Suyu, S. H., Auger, M. W., et al. 2017, MNRAS, 465, 4895

Appendix A: Full joint posterior distribution

We show in Fig. A.1 all mass model parameters sampled for our lens models. All parameters are significantly better constrained by including the extended surface brightness of SN H0pe host galaxy.

Appendix B: Reconstructed SN host in multiple JWST bands

In Sect. 3.2 we obtained an improved lens model using the F200W data and including the extended SN H0pe arc as extra constraints. In Fig. B.1 we show the reconstructed extended host surface brightness in six NIRCam filters, fixing the lens model to the best-fit parameters found with F200W.

We note that while the arc is fitted reasonably well in all bands, especially in bluer ones, large scale patterns in the residuals still remain. Part of these residuals are caused by foreground light contamination from cluster members, in particular from the brightest galaxy at the top left of Fig. 1, which is not included in our model. A second origin of residuals may be due to the mass model being too simplistic, which does not accurately reproduce the magnification of the two southernmost images of the arc (one appears over-magnified, while the other seems under-magnified). Both of these effects—foreground light and mass distribution—will be the focus of a future paper using the modeling approach of [Galan et al. \(2024\)](#).

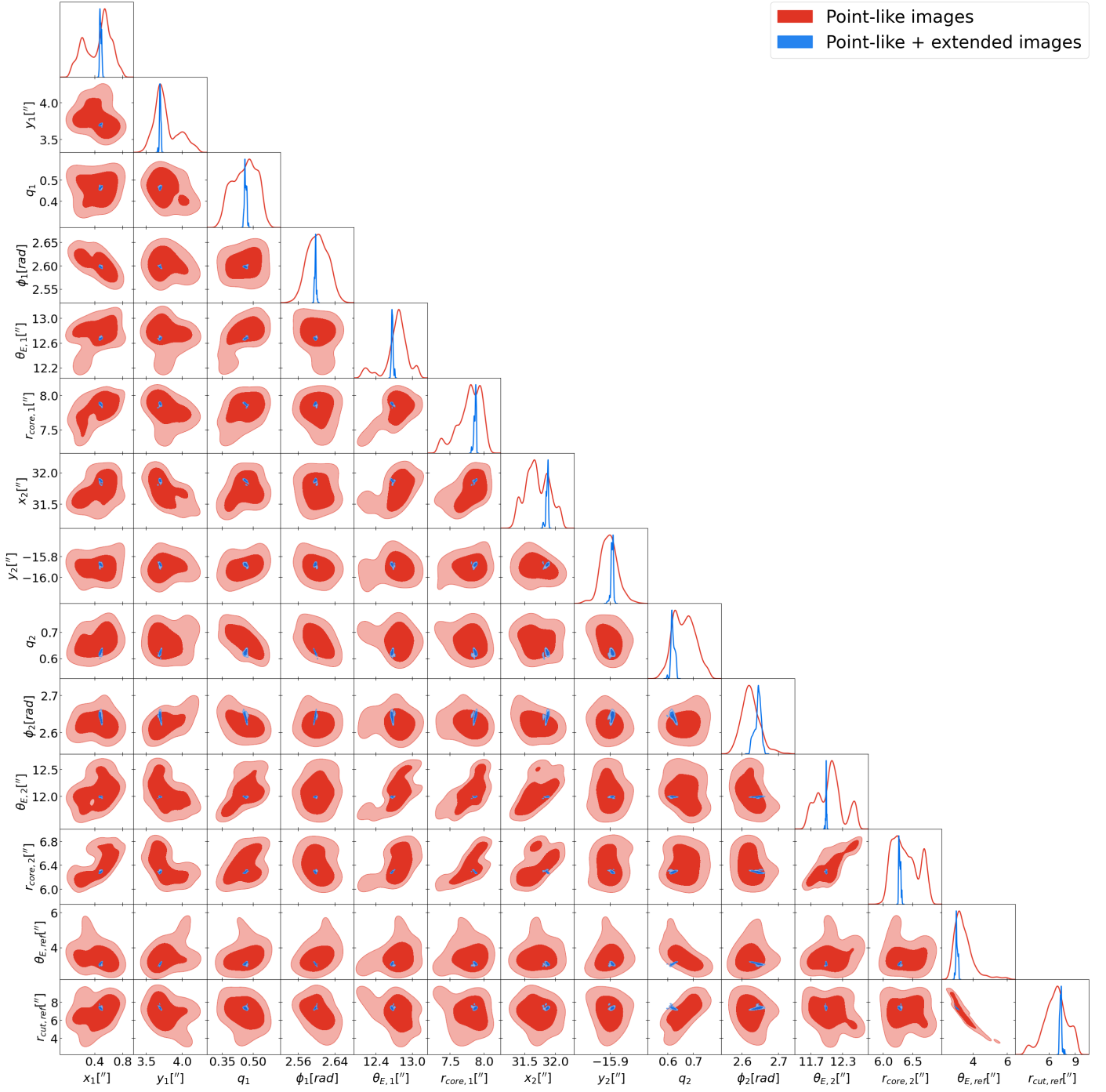


Fig. A.1. Corner plot for all mass parameters for the two cluster scale components and scaling relations of the cluster members. Contours are the 68% and 95% confidence levels for the model using only the positions of the point-like multiple images in red and the full surface brightness of SN H0 host galaxy in blue.

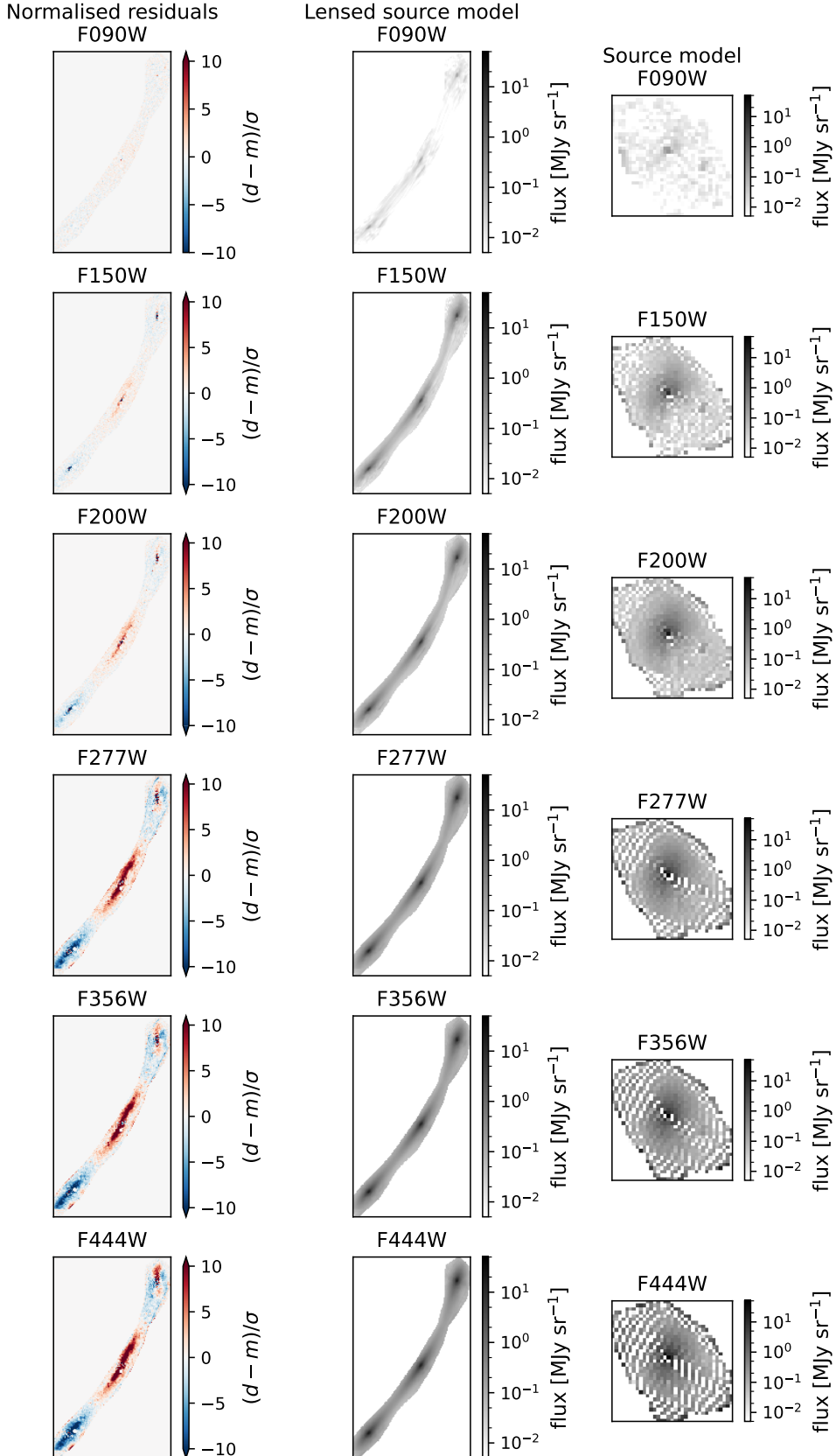


Fig. B.1. Extended SN H0pe host reconstruction in six JWST/NIRCam bands. Our lens model parameters are constrained using F200W only (third row). Subsequently, other bands were used to reconstruct the source surface brightness, fixing the best-fit mass parameters. Normalized residuals (left column) are defined as data – model divided by the uncertainty in each pixel.